Supplementary Information

Study of the thermal stability of studtite by *in situ* Raman spectroscopy and DFT calculations

F. Colmenero[a], L.J. Bonales[b], J. Cobos[b], V. Timón[a]

[a]*Instituto de Estructura de la Materia, CSIC. C/ Serrano, 113. 28006 Madrid, Spain*

[b]*Centro de Investigaciones Energéticas, Medioambientales y Tecnológicas, CIEMAT. Avda/ Complutense, 40. 28040 Madrid, Spain*

Appendix A. Home-made cell

A very simple home-made cell had been used to perform the *in situ* Raman measurements of studtite in contact with liquid water. This cell is composed by two borosilicate glass cover slides of 22 mm diameter and 0.25 mm thickness separated by an O-ring of 20 mm diameter. See Fig. A1

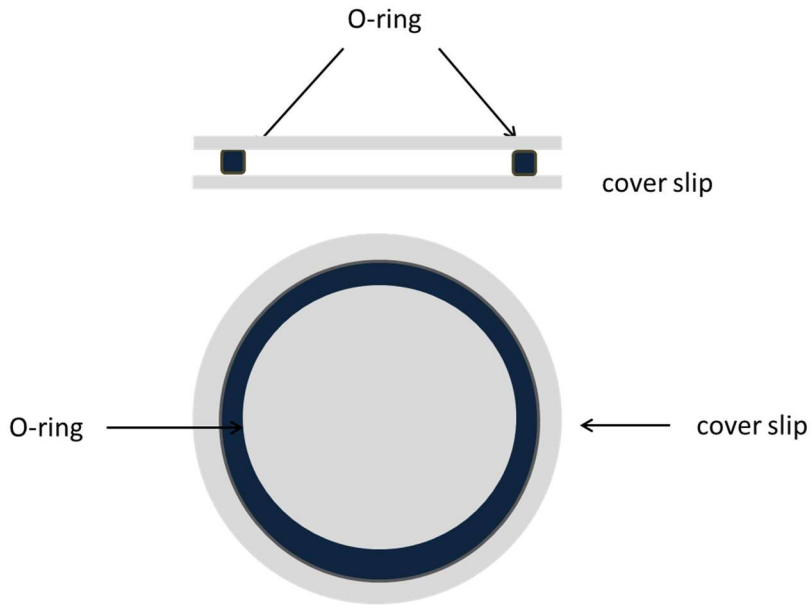

Fig. A1. Home-made cell sketch.

In Figure A.2 the setup it is shown. First, (1) we place an O-ring on top of a cover slip, then some milligrams (10-20 mg) of the solid sample is disposed on the surface of a cover slide provided with the O-ring, and a few drops of water are added over the solid

(2) and, finally, the other cover slide was placed on the top the sample (studtite and water) (3). Therefore, the sample was housed between the two cover slides, separated by the O

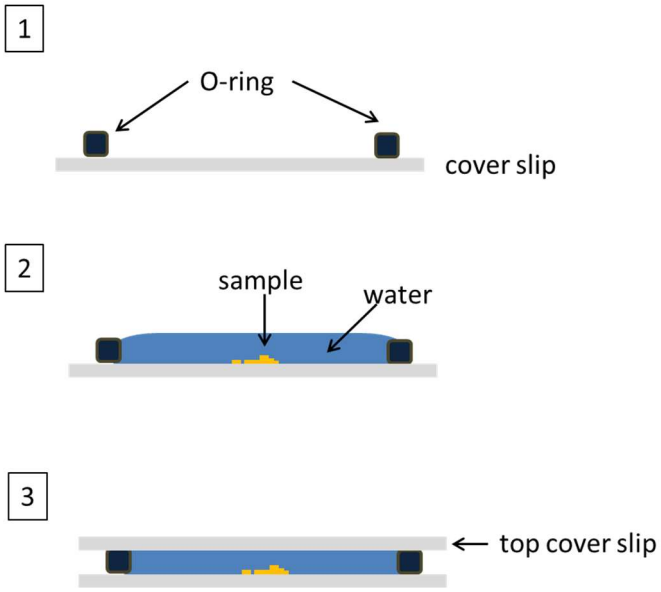

Fig. A2. Home-made cell setup.

Appendix B. Studtite DFT calculations.

The mineral studtite was originally described in 1947 by Vaes [1] as a hydrated carbonate of uranium from a qualitative chemical analysis. Subsequent chemical and powder XRD investigations by Walenta [2] demonstrated that mineral studtite is identical to synthetic $(UO_2)O_2 \cdot 4H_2O$ [3-6]. Subsequent analyses of studtite from the type locality (Shinkolobwe) by Cejka et al. [7] confirmed Walenta's unit-cell determination. The structure of studtite was finally reported in 2003 by [8], which showed that its unit cell is approximately twice the size of the previously accepted unit-cell. The structure is displayed in Fig. B.1. Equilibrium structure is monoclinic and crystallizes in the space group C2/c (Z=4). [9], also reported the thermodynamic stability of the peroxide-containing uranyl minerals.

In studtite, uranium atom displays hexagonal bipyramid coordination. Two oxygen atoms are in apical positions forming with uranium atom nearly linear uranyl UO_2^{2+} uranyl ions. The six equatorial oxygen atoms are two peroxo groups (four oxygen atoms) forming opposite edges of the hexagon and two water molecule oxygen atoms. The different bipyramids are linked by sharing the peroxo equatorial edges and form zig-zag chains along [001] direction.

Most uranyl minerals including uranium as the only high-valence cation invariably contain sheets. However, some minerals as studtite are not based upon sheet of uranyl polyhedra, but contain polymerized uranyl polyhedra in only one dimension. The occurrence of chains rather sheets in U(VI) minerals is usually due to distortions in the polyhedra [10]. The presence of peroxide at the equatorial positions of the uranyl polyhedra results in distorted hexagonal bipyramids, with the peroxide O–O edge length (about 1.46 Å) being much shorter than the typical O–O edge length in uranyl

hexagonal bipyramid (about 2.4 Å) This distortion may prevent the formation of two-dimensional layer structures.

The chains are held together by means of a network of hydrogen bonds. The hydrogen bond structure is show in detail in Fig. B.2. Each water molecule forming part of the uranyl polyhedra (structural water, also called terminal aqua groups) donate two hydrogen bonds with other water molecules which do form part of the bipyramids (crystallization water). The last two molecules participate in four hydrogen bonds. They are acceptors of two hydrogen bonds donated by structural water molecules of two subsequent bipyramids of a chain and are donors of two hydrogen bonds, one with a uranyl oxygen atom and one with a peroxide oxygen atom. These oxygen atoms belong to upper and lower chains. The uranyl oxygen atom is acceptor of one hydrogen bond and the two oxygen atoms in a peroxide group are each one also acceptors of one hydrogen bond. Thus, the network of hydrogen bonds enforces the structure by linking the chains at the same height and upper a lower chains. In studtite two subsequent bipyramids are linked not only by sharing a peroxo O-O edge but also through hydrogen bonds with an intermediate molecule outer of the bypiramids. The outer molecule receives these hydrogen bonds and donates hydrogen bonds to upper and lower chains.

Since there are two kinds of water molecules in the structure, one half being the structural ones and the other crystallization water molecules, the structure is more correctly formulated as $[(UO_2)O_2(H_2O)_2]\cdot 2H_2O$. Due to the fact that peroxo groups are side-bonded (η^2) to the uranium atoms, the structure is commonly referred to as $[(UO_2)(\eta^2\text{-}O_2)(H_2O)_2]\cdot 2H_2O$. However, the notation $[(UO_2)(\mu^2\text{-}O_2)(H_2O)_2]\cdot 2H_2O$ may also be used, indicating that peroxo atoms are μ^2-bridging between symmetry related uranium metal centers.

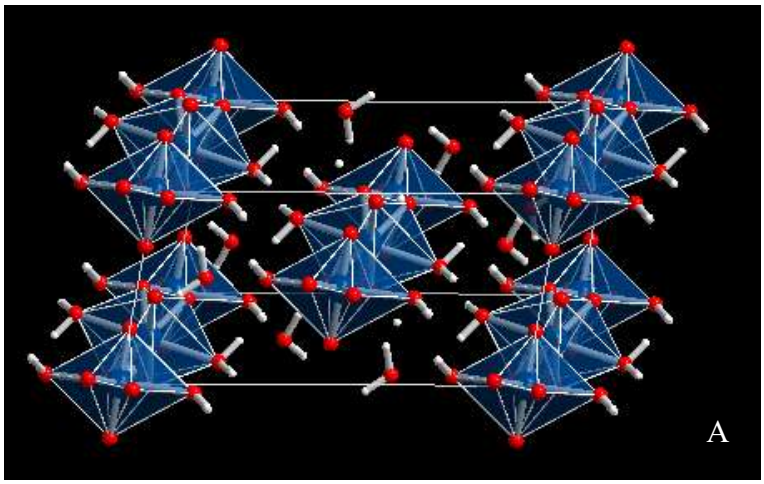
A

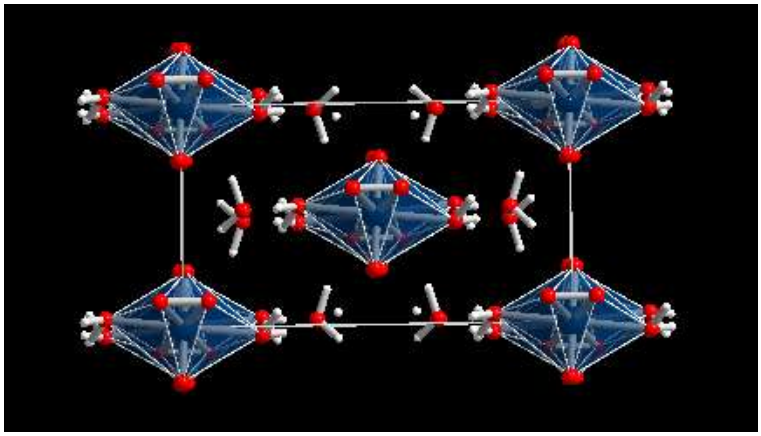

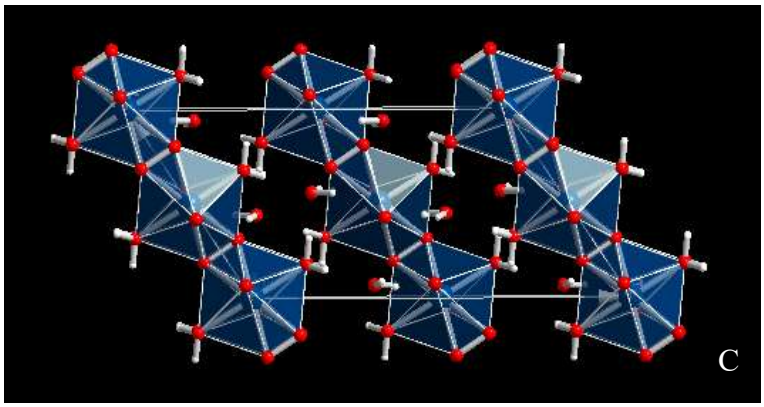
C

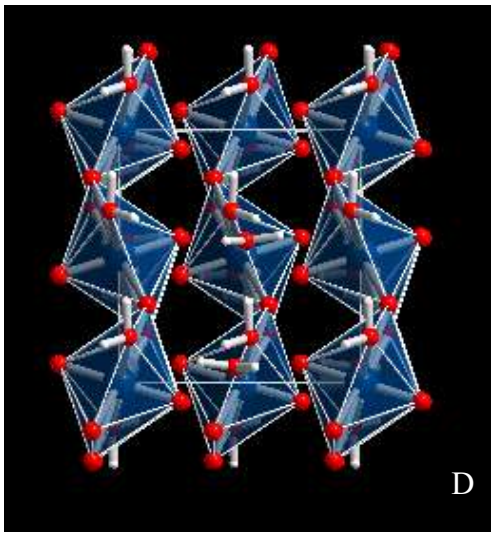

Fig. B.1. Structure of studtite, $(UO_2)(O_2)\cdot 4H_2O$: a) General view of the studtite structure; b) view from [001]; c) view from [010]; d) view from [100]. Color code: U-Blue, O-Red, C-Carbon.

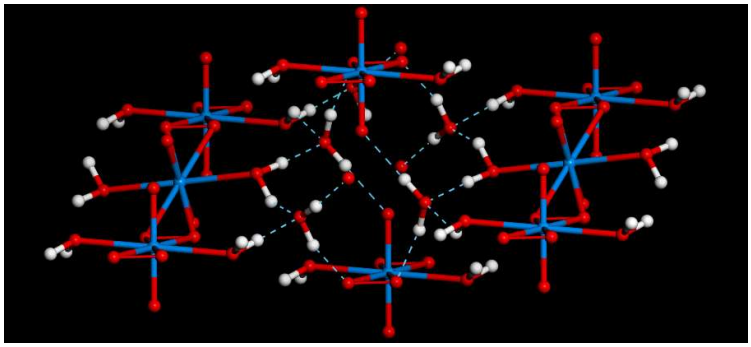

Fig. B.2. Detailed view of the hydrogen bond structure of studtite.

In this work, studtite structure was optimized in the calculations by increasing the different parameters (larger kinetic energy cutoffs and K meshes), i.e., increasing complexity. The optimization performed with a cutoff of 1000 eV and a K mesh of 2 x 4 x 4 (8 K points) gave a well converged structure and was used to determine the final material properties. Calculated lattice parameters, volumes and densities compared with the results of other calculations and the experimental results are given in table 2 of the main part of this paper. The corresponding bond distances and angles are given in

Tables B.1 and B.2. Present results are comparable in accuracy with those of Weck et al. [11, 12].

Table B.1. Studtite bond angles (in deg).

Bond	**Exp.** [8]	**This work**	**DFT** [11]
U1-O1	1.769	1.807	1.83
U1-O2	1.769	1.807	1.83
U1-O3	2.352	2.383	2.38
U1-O3’	2.365	2.395	2.38
U1-O4	2.395	2.400	2.41
U1-U1	4.214	4.248	4.21
O3-O3’	1.464	1.430	1.46
O4-H1	0.978	0.999	1.00
O4-H2	0.975	1.000	1.00
H1..OH2	1.722	1.647	1.62
H2..OH2	1.959	1.644	1.66
O3..H2O	1.757	1.771	1.71
O2..H2O	1.956	1.795	1.79

Table B.2. Studtite bond angles (in deg).

Bond angle	**Exp.** [8]	**This work**	**DFT** [11]
O1-U1-O2	180.0	180.0	180.0
O1-U1-O3	89.73	89.00	88.2
O1-U1-O4	86.53	88.71	86.5
O2-U1-O3	90.27	90.54	92.3
O2-U1-O4	93.47	91.00	87.7
O3-U1-O3’	36.17	34.84	35.5
O3-U1-O3’’’	180.0	180.0	180.0
O3-U1-O3’’’’	143.83	145.16	144.4
O3-U1-O4	71.32	72.53	71.4
U1-O3-U1’’	126.60	125.52	124.0
O4-U1-O3’	107.25	107.35	106.9
O4-U1-O4’	180.0	180.0	180.0
O1-U1-U1’-O1’’	5.99	0.00	0.2

The powder X-ray powder spectrum of studtite was computed from the experimental and computed structures [13]. The most intense lines are compared in Fig. B.3 and, as can be seen, the agreement in line positions and intensities is very good. The use of spectra derived directly from the experimental and computed structures allows for a fair comparison of the results free of interferences as the experimental conditions or possible

artifacts as the presence of sample impurities since both are determined under the identical conditions. Nevertheless, agreement with the experimental pattern of Debets [6] (see also [2] is also good. The main results are given in Table B.3. The pattern computed with program REFLEX, a module of Materials Studio package [14], is given in the main part of this paper.

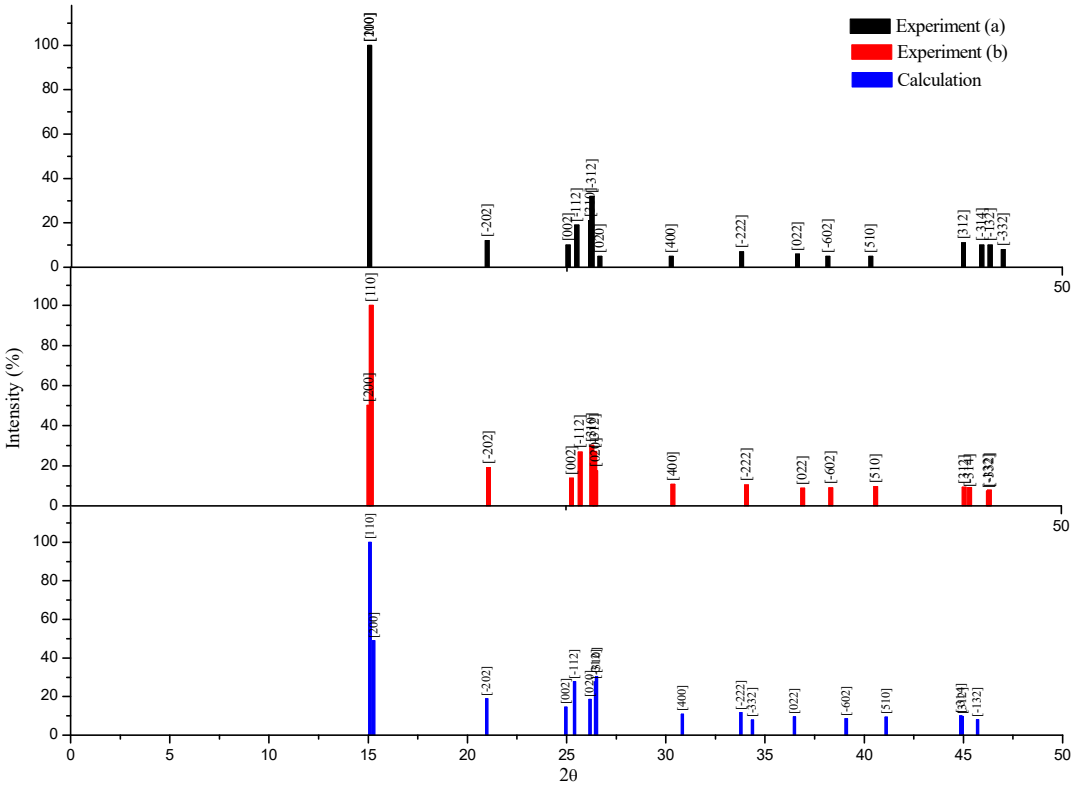

Fig. B.3. X-ray powder spectrum of studtite using CuK_{α} radiation: a) Experimental spectrum [6]; b) X-ray powder spectrum computed form experimental geometry [8]; c) X-ray powder spectrum computed from calculated geometry.

Table B.3. Main reflections in the X-ray powder spectrum of studtite. The experimental data are from a synthetic sample [6]

	Experimental reflections			Calculated reflections (Experimental geometry)			Calculated reflections (Calculated geometry)		
2θ	d(Å)	I (%)	hkl	2θ	d(Å)	I (%)	2θ	d(Å)	I (%)
15.055	5.88	100	200	15.067	5.8753	50.252	15.276	5.7955	48.977
15.055	5.88	100	110	15.174	5.8341	100.0	15.087	5.8675	100.0
20.984	4.23	12	-202	21.102	4.2067	19.182	20.971	4.2327	18.937
25.063	3.55	10	002	25.282	3.5198	13.810	24.960	3.5645	14.485
25.501	3.49	19	-112	25.723	3.4605	26.910	25.395	3.5045	27.734
26.188	3.40	21	310	26.314	3.3841	30.183	26.509	3.3597	30.472
26.267	3.39	32	-312	26.460	3.3658	27.202	26.465	3.3651	27.537
26.667	3.34	5	020	26.502	3.3605	17.568	26.175	3.4018	18.623
30.272	2.95	5	400	30.403	2.9376	10.744	30.832	2.8978	10.927
33.823	2.648	7	-222	34.121	2.6256	10.455	33.777	2.6516	11.681
36.634	2.451	6	022	36.953	2.4306	8.821	36.481	2.4610	9.587
38.167	2.356	5	-602	38.361	2.3446	9.070	39.096	2.3022	8.485
40.339	2.234	5	510	40.636	2.2184	9.721	41.102	2.1943	9.367
45.020	2.012	11	312	45.095	2.0089	9.365	44.949	2.0150	9.713
45.935	1.974	10	-314	45.368	1.9974	9.246	44.867	2.0185	10.023
46.358	1.957	10	-132	46.312	1.9589	7.398	45.711	1.9832	8.074
47.019	1.931	8	-332	46.362	1.9569	7.822	46.362	1.9569	7.822

Appendix C. Raman modes of studtite.

Fig. C.1. The atomic motions associated to Raman active vibrational normal modes of studtite.

Mode 3319 cm^{-1} – ν(OH) – OH stretching for crystallization H_2O molecules

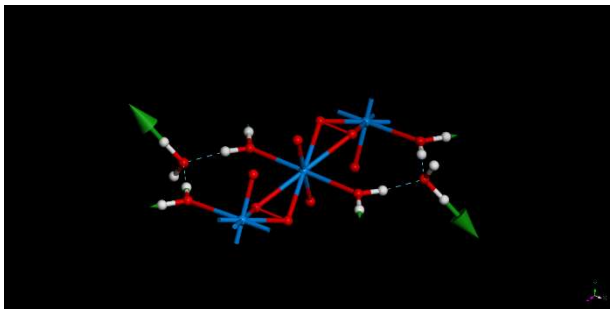

Mode 3238 cm^{-1} – ν(OH) – OH stretching for crystallization H_2O molecules

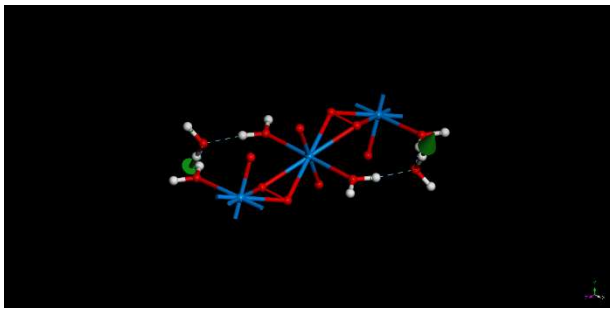

Mode 3033 cm^{-1} – ν(OH) – OH stretching for structural H_2O molecules

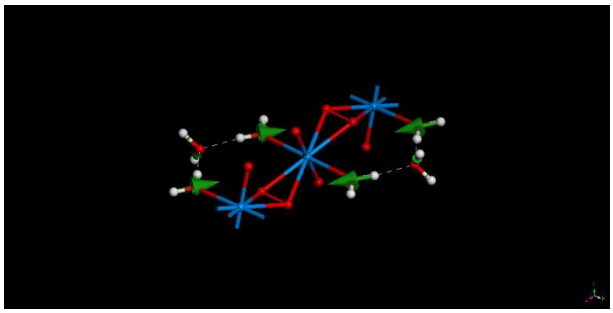

Mode 2970 cm^{-1} – ν(OH) – OH stretching for structural H_2O molecules

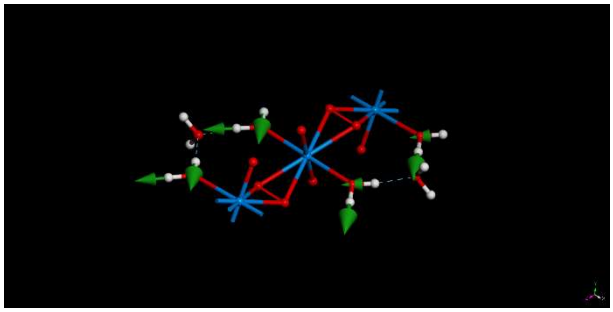

Mode 1679 cm^{-1} – δ(H_2O) – H_2O bending for structural H_2O molecules

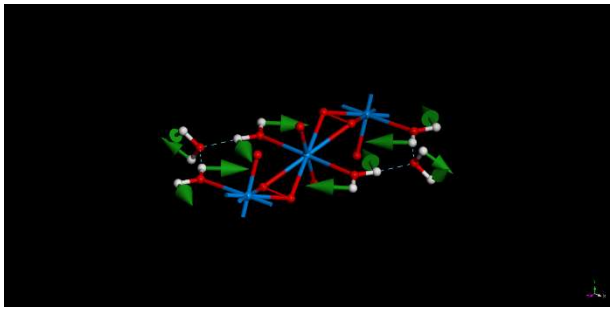

Mode 1638 cm^{-1} – δ(H_2O) – H_2O bending for crystallization H_2O molecules

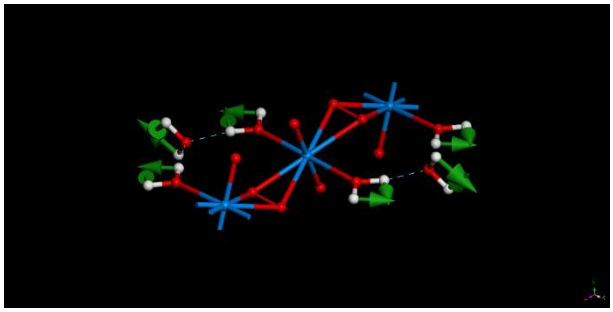

Mode 917 cm^{-1} – ν(OO) – Peroxo O-O stretching

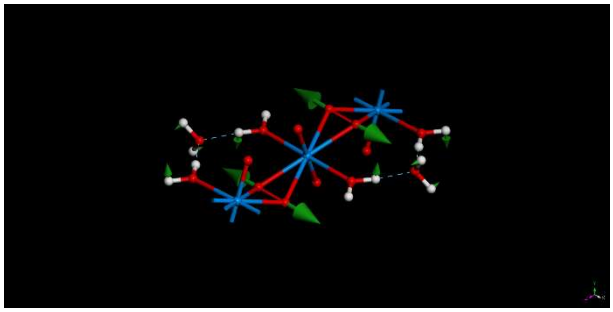

Mode 798 cm^{-1} – $\nu^s(UO_2^{2+})$ – Symmetric UO_2^{2+} stretching

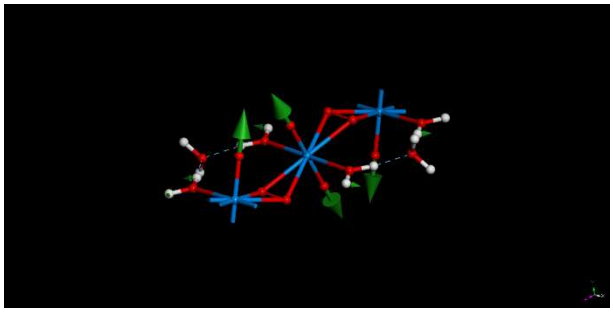

Mode 686 cm^{-1} – $\rho(H_2O\text{-st.})+ \omega(H_2O\text{-cr.})$ – H_2O librations. Rocking vibrations for structural H_2O molecules and wagging vibrations for crystallization H_2O molecules

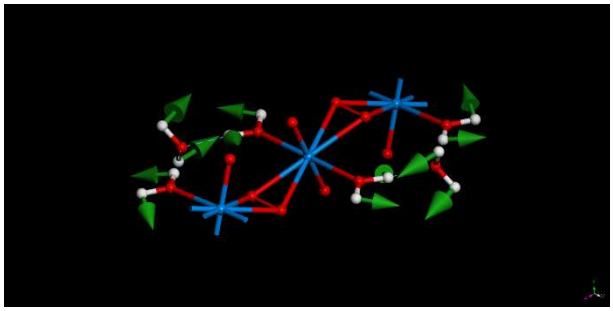

Mode 446 cm^{-1} – $\nu^s(UO_{aqua})$ – Symmetric UO_{aqua} stretching (H_2O-str. translation)

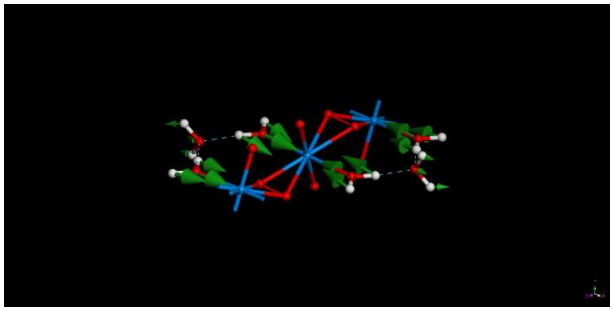

Mode 402 cm^{-1} – $\rho(OUO_{perox})$ – OUO_{perox} rocking

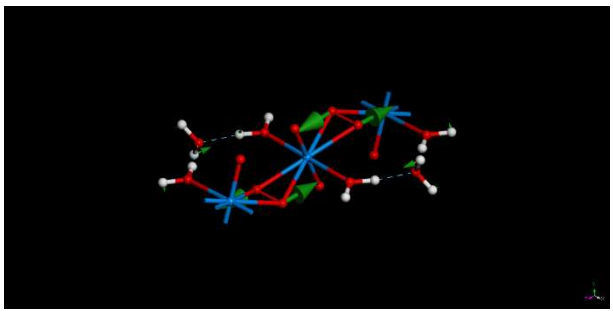

Mode 372 cm^{-1} – $\rho(OUO_{perox})$ – OUO_{perox} rocking

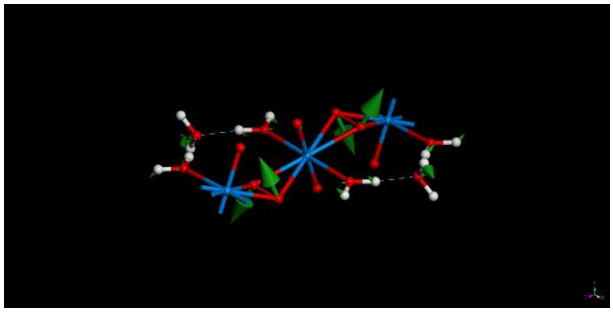

Mode 309 cm^{-1} – $\rho(OUO_{aqua})$+T(H_2O-cr.) – OUO_{aqua} rocking plus crystallization H_2O translation

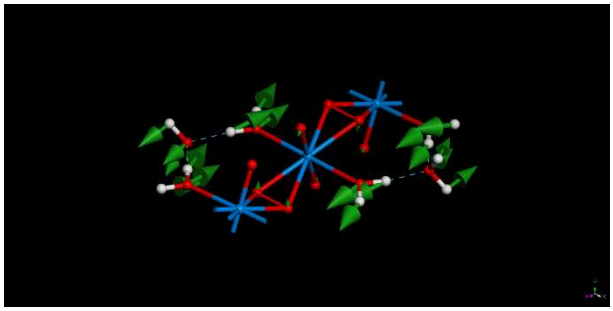

Mode 307 cm^{-1} – $\rho(OUO_{perox})$ – OUO_{perox} rocking

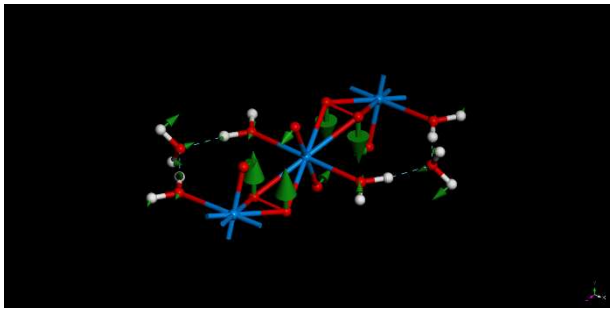

Mode 256 cm^{-1} – $\rho(UO_2^{2+})$+ $\rho(OUO_{aqua})$+$\rho(OUO_{perox})$+T(H_2O-cr.) – Uranyl, OUO_{aqua}, and OUO_{perox} rocking plus crystallization H_2O molecules translation

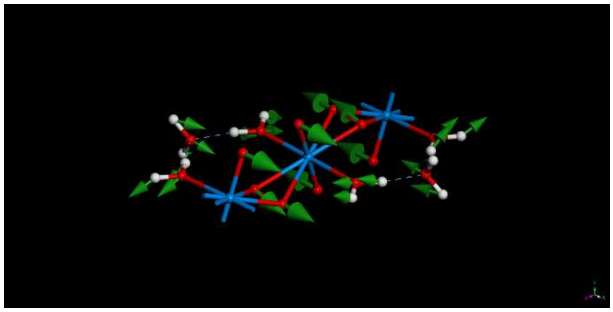

Mode 247 cm^{-1} – $\rho(UO_2^{2+})$+ $\rho(OUO_{aqua})$+$T(H_2O\text{-cr.})$ – Uranyl and OUO_{aqua} rocking plus crystallization H_2O molecules translation

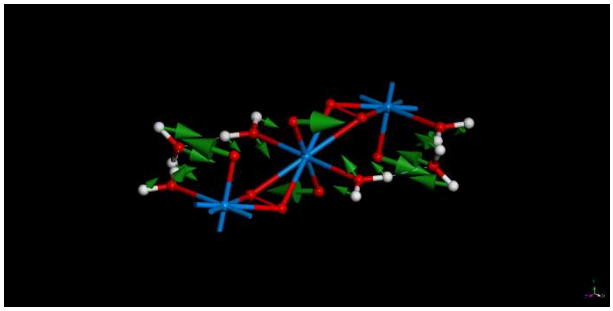

Mode 223 cm^{-1} – $\rho(OUO_{aqua})$+$\rho(UO_2^{2+})$+$\rho(OUO_{perox})$ – OUO_{aqua}, OUO_{perox}, and uranyl rocking

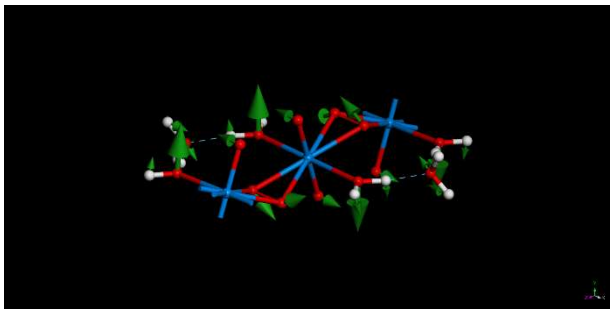

Mode 213 cm^{-1} – $\rho(UO_2^{2+})$+ $\rho(OUO_{aqua})$+$T(H_2O\text{-cr.})$ – Uranyl and OUO_{aqua} rocking plus crystallization H_2O molecules translation

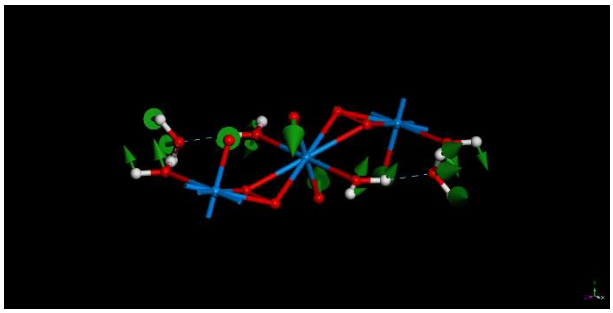

Mode 185 cm^{-1} – $\rho(UO_2^{2+})$+ $\rho(OUO_{aqua})$+$\rho(OUO_{perox})$+$T(H_2O\text{-cr.})$ – Uranyl, OUO_{aqua}, and OUO_{perox} rocking plus crystallization H_2O molecules translation

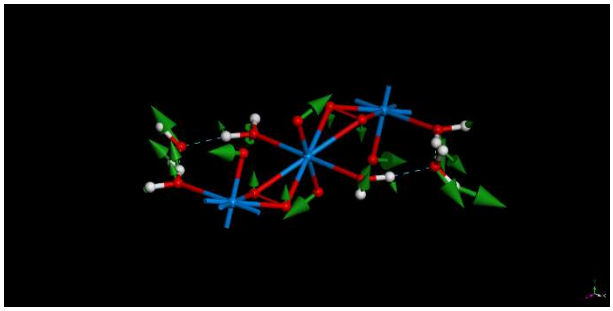

Mode 179 cm^{-1} – $\rho(UO_2^{2+})$ – uranyl UO_2^{2+} rocking

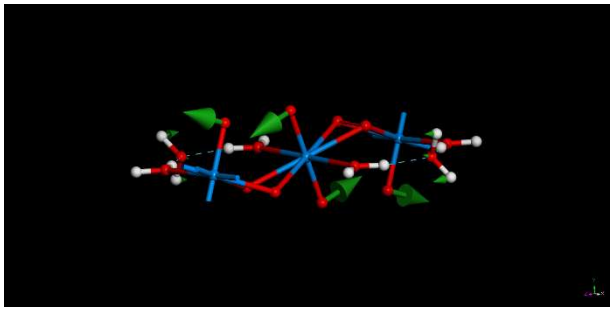

Mode 163 cm^{-1} – $T(H_2O\text{-cr.})$ – crystallization H_2O molecules translation

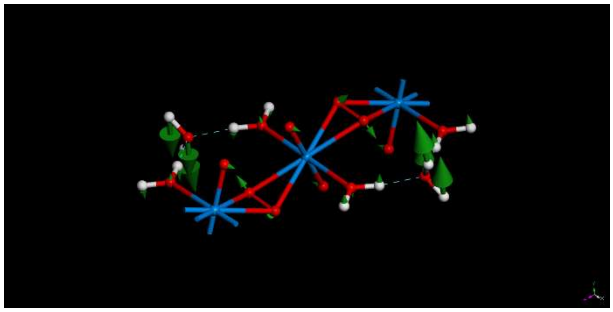

Mode 154 cm^{-1} – $\rho(OUO_{aqua})$+$\rho(UO_2^{2+})$+$\rho(OUO_{perox})$+$T(H_2O\text{-cr.})$ – $OUO_{aqua,}$, OUO_{perox}, and uranyl rocking plus crystallization H_2O molecules translation

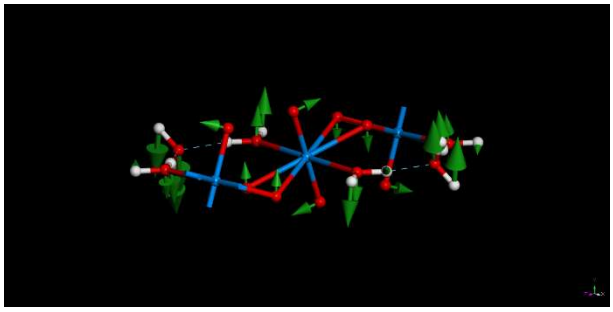

Mode 135 cm^{-1} – $\rho(OUO_{aqua})+\rho(UO_2^{2+})+T(H_2O\text{-cr.})$ – OUO_{aqua} and uranyl rocking plus crystallization H_2O molecules translation

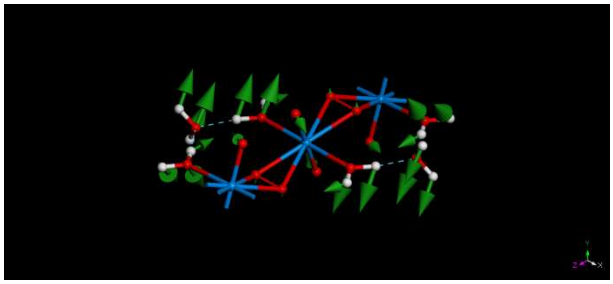

Mode 101 cm^{-1} – $\rho(OUO_{aqua})+\rho(UO_2^{2+})+T(H_2O\text{-cr.})$ – OUO_{aqua} and uranyl rocking plus crystallization H_2O molecules translation

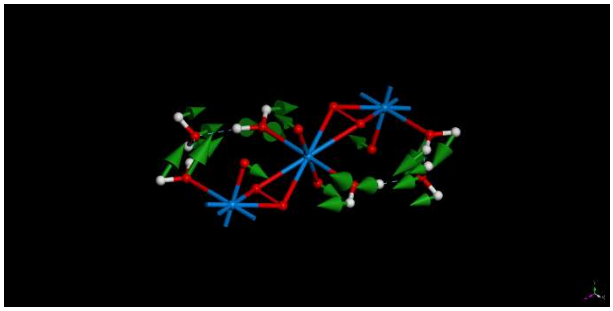

References

[1] J.F. Vaes, Six nouveaux min´eraux d'urane provenant de Shinkolobwe (Katanga), Ann. Soc. Geol. Belg. , 70 (1947) B212–B229.

[2] K. Walenta, On Studtite and lts Composition, Am. Mineral., 59 (1974) 166–171.

[3] T. Sato, Thermal decomposition of uranium peroxide hydrate, Naturwissenschaften, 48 (1961) 693-693.

[4] T. Sato, Uranium peroxide hydrates, Naturwissenschaften, 48 (1961) 668-668.

[5] T. Sato, Preparation of uranium peroxide hydrates, J. Appl. Chem., 13 (1963) 361-365.

[6] P.C. Debets, X-ray diffraction data on hydrated uranium peroxide, J. Inorg. Nucl. Chem., 25 (1963) 727-730.

[7] J. Cejka, J. Sejkora, M. Deliens, New data on studtite, $UO_4 \cdot 4H_2O$, from Shinkolobwe, Shaba, Zaire, Neues Jahrbuch fuer Mineralogie, Monatshefte, 3 (1996) 125–134.

[8] P.C. Burns, K.-A. Hughes, Studtite, $[(UO_2)(O_2)(H_2O)_2](H_2O)_2$: The first structure of a peroxide mineral, Am. Mineral., 88 (2003) 1165-1168.

[9] K.-A.H. Kubatko, K.B. Helean, A. Navrotsky, P.C. Burns, Stability of Peroxide-Containing Uranyl Minerals, Science, 302 (2003) 1191-1193.

[10] I. Grenthe, J. Drożdżyński, T. Fujino, E.C. Buck, T.E. Albrecht-Schmitt, S.F. Wolf, Uranium, in: The chemistry of the actinide and transactinide elements, Springer Netherlands, 2008, pp. 253-698.

[11] P.F. Weck, E. Kim, C.F. Jove-Colon, D.C. Sassani, Structures of uranyl peroxide hydrates: a first-principles study of studtite and metastudtite, Dalton Trans., 41 (2012) 9748-9752.

[12] P.F. Weck, E. Kim, E.C. Buck, On the mechanical stability of uranyl peroxide hydrates: implications for nuclear fuel degradation, RSC Adv., 5 (2015) 79090-79097.

[13] R.T. Downs, K.L. Bartelmehs, G.V. Gibbs, M.B. Boisen, Interactive software for calculating and displaying X-ray or neutron powder diffractometer patterns of crystalline materials, Am. Mineral., 78 (1993) 1104-1107.

[14] MaterialsStudio, http;//accelrys.com/products/materials-studio, (2014).